Association of phosphorylation site of tau protein with neuronal apoptosis in Alzheimer's disease

著者	Kobayashi Katsuji, Nakano Hiroyuki, Hayashi Masahiro, Shimazaki Masao, Fukutani Yuken, Sasaki Kazuo, Sugimori Kaoru, Koshino Yoshifumi
journal or publication title	Journal of the Neurological Sciences
volume	208
page range	17-24
year	2003-04-01
URL	http://hdl.handle.net/2297/1795

Association of phosphorylation site of tau protein with neuronal apoptosis in Alzheimer's disease

Katsuji Kobayashi [1], Hiroyuki Nakano [1], Masahiro Hayashi [2], Masao Shimazaki [1], Yuken Fukutani [3], Kazuo Sasaki [3], Kaoru Sugimori[1], Yoshifumi Koshino [1]

[1] Department of Psychiatry and Neurobiology, Graduate School of Medical Sciences, Kanazawa University, 13-1, Takara-machi, Kanazawa, 920-8641, Ishikawa-ken, Japan,
[2] National Sanatorium Hokuriku Hospital, Nobusue, Jouhana-machi, Toyama-ken, Japan
[3] Department of Psychiatry, Fukui Medical University, Matsuoka-tyou, Fukui-ken, Japan.

Address correspondence to:
Katsuji Kobayashi, Department of Psychiatry and Neurobiology, Graduate School of Medical Sciences, Kanazawa University, 13-1, Takara-machi, 920-8641, Kanazawa, Ishikawa-ken, Japan
Telephone +81-76-265-2301
Fax +81-76-234-4254
E-mail kobakatu@med.m.kanazawa-u.ac.jp

Key words:
Neurofibrillary tangles, apoptosis, TUNEL, Alzheimer's disease, pretangle neurons

Abstract
In addition to neuritic changes and amyloid deposits, neuronal and glial cell apoptosis is an important pathological feature of Alzheimer's disease (AD). Several factors have been postulated as causes or triggers of cellular apoptotic change. This study focused on a quantifiable relationship between phosphorylation sites of tau protein in the neurofibrillary tangles (NFT) and neuronal apoptosis. Five monoclonal anti-tau antibodies (AT180, AT8, HT7, Tau2 and Tau5) for NFT labeling and TdT-mediated UTP nick-end labeling (TUNEL) for localizing apoptotic change were employed. TUNEL-stained neuronal nuclei showed significantly high density in the entorhinal cortex, cornu ammonis (CA) and the parietal cortex. In all regions, density of TUNEL-stained neuronal nuclei showed significantly direct correlation with that of AT8-, AT180- and Tau2-positive neurons. Correlation of TUNEL-stained neuronal nuclei with tau-positive neurons differed depending on the cerebral regions. Density of TUNEL-stained neuronal nuclei showed inverse correlation with that of both AT8-positive and Gallyas-stained NFT in the CA and showed significantly direct correlation with AT8- and HT7-positive neurons in the frontal cortex. Density of tau-positive and Gallyas-stained NFT was higher than that of TUNEL-stained nuclei. We conclude that phosphorylation sites of tau, 159-163 and 202-205, are probably associated with neuronal apoptosis and apoptotic change follows abnormal phosphorylation of tau.

Introduction

Apoptosis, a programmed cell death by intrinsic mechanism to regulate cell population, has been shown to occur extensively in brains from patients with Alzheimer's disease (AD). In addition to neurofibrillary tangles (NFT) and beta amyloid protein (BAP) deposits, abundant apoptotic neuronal and glial cells are another pathological hallmark of AD [1-18]. Abnormal phosphorylation of the tau protein that leads to NFT formation, BAP deposits, high concentration of amyloid precursor protein (APP), caspase-3, the presenilin 1 and 2 gene and nitric oxide are considered to be important triggers of neuronal and glial apoptosis [1-25]. Since NFT are present in the neuronal cytoplasm, NFT and neuronal apoptosis have been considered to be intimately associated with each other. To the best of our knowledge, 13 studies, ten in vivo [1, 3, 5, 7, 8-10, 13, 16, 18] and three in vitro [15, 18, 22], have addressed the relationship between NFT formation and neuronal apoptosis. However, it is still unclear whether neuronal apoptosis is a result or cause of abnormal phosphorylation of tau.

Tau immunohistochemistry has differentiated pretangle neurons, known as stage 0 tangles [26-27], from argyrophilic NFT, and phosphorylation sites of the amino acid sequence of tau molecules have been analyzed in AD brains [28-29]. The pretangle neurons are believed to occur in the early stage and may disappear in the late stage of AD with some of them remaining unchanged. A recent study has demonstrated that neurons with normal nuclear morphology, known as type 1 [1], positive for TdT-mediated UTP nick end-labeling (TUNEL) contained abundant hyperphosphorylated tau, but type 2 TUNEL-positive nuclei, loss of nucleolus [1], were shown not to be associated with either NFT or senile plaques [18].

The tau protein consists of 441 amino acid long sequences. AD-associated abnormal phosphorylation of the tau protein occurs at serine 202 and is predominant in the neurites [30]. The phosphorylation site can be detected with AT8 because the phosphorylation site of the amino acid sequence of 202-205 is recognized by AT8 [31-32]. Many anti-tau antibodies have been shown to recognize different sites of abnormal phosphorylation in AD [28-29, 33-34]. Other phosphorylation sites of tau protein are 231 detectable by AT180, 95-108 detectable by Tau2, and 159-163 detectable by HT7. The sites of tau amino acid sequences recognized by Tau5 are not exactly known, but it has been speculated that they are located in the central zone of the tau molecule.

For the study presented here, we performed an immunohistochemical and quantitative study to determine any quantifiable relationship between the phosphorylation site of the tau protein and TUNEL-stained nuclei in AD brains.

Materials and methods

Seven brains from patients with AD and seven controls [25], all of whom met the diagnostic pathological criteria for AD [35-36], were enrolled in this study. The post-mortem delay ranged from 3.0 to 8.4 hours (average 3.7 hours) [25]. The brains removed at autopsy were fixed with 10% formalin, and brain slices were cut coronally and embedded in paraffin wax. Representative hemispheric sections that contained the frontal, temporal, parietal and occipital lobes, hippocampus and basal ganglia were sliced to a thickness of 7μm. Pathologic examination was performed with hematoxylin and eosin (H-E), luxol-fast blue (LFB) and cresyl violet, Holzer and Bodian stains.

Immunohistochemistry employed an avidin-biotin peroxidase complex (ABC) technique (Vectastain ABC kit, Vector Laboratories Inc., Burlingame, USA). To label differently phosphorylated tau proteins, five monoclonal antisera, AT8 (diluted 1:1000), AT180 (diluted 1:2000) and HT7, all purchased from Innogenetics, USA, and Tau 2 (1:400) and Tau 5 (1mg/ml), both purchased from PharMingen International, San Diego, CA, were used. Amyloid deposits were labeled with a monoclonal anti-BAP antiserum (clone 4G8, diluted 1:2000; Sennetek, USA). All sections were heated in a hydrated microwave (750 watts, 60 minutes) following by treatment with a 0.3% hydrogen peroxidase solution for 10 minutes. The sections for BAP labeling were pretreated with a 90% formic acid solution for 5 minutes. The TUNEL technique employed an "ApopTag" in situ apoptosis detection kit (Oncor, Gaithersburg, MD) to label DNA termini in the sections. Sections for TUNEL labeling were first treated with proteinase K (20μg/ml for 2 min at room temperature), and the endogenous peroxidase activity was quenched with 0.3% H_2O_2 for 5min. The working strength TdT enzyme mixture was pipetted onto slide-mounted tissue sections, coverslipped, and incubated for 1h at 37 degrees. The sections were then incubated in a working strength stop/wash buffer for 10 min, incubated with anti-digoxigenin peroxidase conjugate and developed with a diaminobenzidine (DAB)-nickel ammonium solution to which were added a 0.6% nickel ammonium solution, 0.005M imidazole and 0.0002% H_2O_2 in 0.05M TRIS-HCL buffer, pH 7.6). Double immunolabeling of the above-mentioned anti-tau antisera and TUNEL-positive nuclei was performed to confirm the co-localization of the apoptotic nuclei and tau-positive neurons in several sections. Briefly, the TUNEL-stained sections were processed with tau labeling and developed with DAB solution. The materials stained during TUNEL turned dark blue and those during the tau labeling brown. Brain sections were also stained with the Gallyas silver impregnation technique to assess neuropathological staging [37].

Quantitative method

Four hemispheric coronal sections were prepared to localize the counting areas for TUNEL and Gallyas staining and tau labeling. The first section was prepared for examination of the lateral prefrontal cortex and was defined as the section through the temporal pole, and the second section as the section through the lateral geniculate body, containing the temporal neocortex, entorhinal cortex and the sector 1-4 of the cornu ammonis (CA). The third section for examination of the parietal cortex was defined as the section through the precuneus, and the fourth section for examination of the occipital cortex as the section through Gennari's line.

For quantification of the tau-labeled, TUNEL- and Gallyas-stained cells, the cells were viewed with a Nikon Eclipse E600, and the images captured with a Polaroid Microscopic Camera (Polaroid Corporation, Cambridge, MA) and displayed with Macintosh Adobe Photoshop 5.0. In each visual field (vf) (X20 objective and X10 eyepiece, 1vf=0.00168 mm^2) printed out in color, the stained cells were counted independently by two of the authors (KK and MH). The density of tau-labeled neurons, Gallyas-stained NFT and TUNEL-positive neuronal nuclei was determined by averaging the densities in five non-overlapping visual fields. Evaluation of the tissue changes and fibrillary gliosis with, respectively, H-E and with Holzer stained preparations has been

described elsewhere [25]. Statistical analysis employed analysis of variance (ANOVA), Student's t-test and Pearson's correlation analysis with Stat View 5.0 and SPSS for Microsoft Windows. Statistical significance was set at $p<0.05$.

Results

With tau and TUNEL double labeling, TUNEL-stained nuclei in the AD brains co-localized more frequently with AT180- and AT8-positive neurons than with neurons positive for the other anti-tau antisera, and many glial nuclei were also stained with the TUNEL technique (Figure 1). However, apoptotic bodies were rarely observed, and condensation of nuclear chromatin only occasionally, while no membrane bleb formation was identified. TUNEL and tau double labeling resulted in a reduced intensity of tau immunoreactivity compared with single labeling with either. AT180 and AT8 labeling appeared to be most sensitive for visualization of neuritic threads. Tau2 and Tau5 frequently labeled not homogeneous but coiled- or tangle-shaped NFT. BAP labeling with 4G8 antiserum revealed abundant deposits of BAP and tau labeling and the Gallyas technique a sufficient number of senile plaques to fulfill the pathological criteria for AD [35-36]. Technical difficulties with double staining with the TUNEL and Gallyas techniques made it impossible to determine any co-localization of Gallyas-stained NFT and TUNEL-stained nuclei. Control brains contained hardly any TUNEL-stained cells and tau immunolabeling showed a limited number of positive neurons in the entorhinal cortex, CA and temporal cortex. 4G8 labeling showed only diffuse, non-neuritic plaques in the cerebral cortex, which did not fulfill the AD diagnostic pathological criteria [35-36]. The absence of TUNEL-stained neurons in control brains made it impossible to perform a comparative analysis of correlation between TUNEL and tau labeling in AD brains and that in the control brains. The anti-tau antisera diffusely labeled neuronal cell bodies and visualized neuritic threads and dystrophic neurites around the neuritic plaques. With the Gallyas technique, NFT were accentuated in the entorhinal cortex, CA and occipito-parietal cortex, a phenomenon compatible with stage-related NFT involvement in AD [25, 37].

In the AD brains, there was no statistical difference in the error variance density of neurons positive for five anti-tau antisera (AT180: $p=0.009$, AT8: $p=0.022$, HT7: $p=0.003$, Tau2: $p=0.0001$, Tau5: $p=0.001$), Gallyas-stained NFT ($p=0.0001$) and TUNEL-positive neuronal nuclei ($p=0.0001$) among the AD cases examined.

The density of TUNEL-stained neuronal nuclei, expressed as mean value (mean) $\pm$ standard deviation (S.D), in the seven cerebral regions showed region-specific distribution (Figure 2), and the results of statistical analysis with two-tailed Student's t-test are shown in Table 1 TUNEL. The frontal cortex showed a density of 1.1 ± 1.4 (mean $\pm$ S.D), which was significantly lower than the density of the other cerebral regions (CA: $t=8.646$, $p<0.0001$; entorhinal cortex: $t=5.988$, $p<0.0001$; cingulate: $t=8.821$, $p<0.0001$; temporal: $t=4.734$, $p<0.0001$; parietal: $t=6.891$, $p<0.0001$; occipital: $t=7.138$, $p<0.0001$). The density of TUNEL-stained neurons was 11.5 ± 6.4 in the entorhinal cortex, 9.0 ± 4.1 in the parietal cortex, 8.6 ± 3.3 in the CA and 8.6 ± 4.7 in the occipital cortex. The two highest t values were detected in following pairs: $t=8.821$ between the frontal cortex and the cingulate cortex, and $t=8.646$ between the frontal cortex and the CA. For these four regions, GML multivariate analysis demonstrated that TUNEL-stained neuron density of

the occipital cortex was significantly higher than that of the CA ($p=0.001$), and that the CA had a higher density of TUNEL-stained neurons than did the frontal ($p=0.0001$) or cingulate cortex ($p=0.004$). No significant difference was found between the CA and entorhinal cortex. The entorhinal cortex had a significantly high density of Gallyas-stained NFT and AT8-positive neurons.

Regional differences in density of neurons positive for the five anti-tau antisera and Gallyas-stained NFT were analyzed with the unpaired t-test and many significant differences in density of labeled neurons among the cerebral regions. The rough estimate of the distribution pattern, represented by the of shaded box for insignificant t values and the open boxes for significant t values in Table 1, indicates that the pattern for TUNEL-stained neuron density was quite different from that for neurons labeled with other methods, that is, the former featured an absence of significant differences in the density of labeled neurons between the CA and entorhinal cortex. Density distribution pattern of neurons positive for AT8 (Table 1 AT8) and AT180 (Table 1 AT180) were very similar to each other, and it is likely that Tau2 (Table 1 Tau2) and Tau5 (Table 1 Tau5) roughly labeled Gallyas-stained NFT (Table 1 Gallyas). Fewer significant pairs were observed for HT7 labeling than for the other labeling methods (Table 1 HT7).

Pearson's correlation analysis of the average density in all regions of total neurons positive for the five anti-tau antisera, TUNEL-stained neuronal nuclei and Gallyas-stained NFT showed that TUNEL-stained neuronal density correlated positively with that of neurons positive for AT8 ($r=0.210$, $p=0.011$), Tau2 ($r=0.175$, $p=0.037$) and AT180 ($r=0.175$, $p=0.037$). Correlation analysis of the seven regions showed an inverse correlation between the density of TUNEL-stained neurons and that of AT8-positive ($r=-0.702$, $p=0.0001$) and Gallyas-stained NFT ($r=-0.562$, $p=0.001$) in the CA as well as that of AT180-positive neurons ($r=-0.430$, $p=0.018$) in the temporal neocortex. In contrast, TUNEL-stained neuronal density correlated positively with the density of AT8-positive neurons ($r=0.556$, $p=0.039$), HT7 ($r=0.555$, $p=0.040$) and Tau5 ($r=0.579$, $p=0.005$) in the frontal neocortex and Tau5 ($r=0.818$, $p=0.004$) in the occipital cortex. There was no statistical correlation in density between TUNEL-stained neurons and tau-positive or Gallyas-stained NFT in the cingulate gyrus, entorhinal cortex or parietal cortex.

The ratio of neurons labeled with each of the anti-tau antisera to the TUNEL-labeled nuclei was 26.5% for AT180, 28.9%for AT8, 36.9% for HT7, 81.2% for Tau2, 40.7% for Tau5 and 22.8% for Gallyas technique, shown in Figure 3. The ratios of Tau2-labeled neurons to TUNEL-labeled neurons were markedly high, ranging from 26% to 81%, in the CA, entorhinal cortex, temporal cortex, cingulate cortex and parietal cortex.

Discussion

Post-mortem delay in our AD cases, which ranged from 3.0 to 8.4 hours, was found to make only a minor contribution to an increase in apoptotic cells [25, 38]. Regional density of tau-positive neurons, Gallyas-stained NFT and TUNEL-stained neuronal nuclei showed no statistically significant differences among the AD cases in our study. Therefore, inter-case differences in density of NFT and TUNEL-stained neurons among AD cases can be neglected for the purpose of this study.

The density of TUNEL-stained neuronal nuclei was significantly low in the frontal cortex and high in the CA, entorhinal and parieto-occipital cortex. This pattern roughly reflects the stage-related NFT involvement of cerebral regions [37]. Co-localization of tau immunoreactivity and TUNEL-stained nuclei was not observed in the control brains irrespective of the presence of limited numbers of tau-labeled neurons. The absence of TUNEL-stained nuclei in tau-positive neurons in the control brains suggests that cell death in conjugation with the accumulation of abnormally phosphorylated tau does not occur in non-demented individuals.

Our study confirmed the presence of TUNEL-labeled nuclei in tau-labeled neurons. Because of the reduced labeling sensitivity in TUNEL and tau double labeling, we were unable to directly count tau-positive neurons with TUNEL-stained nuclei. Although the precise ratio of TUNEL-stained nuclei to tau-positive neurons must thus remain unknown, a certain amount of tau-positive neurons can be regarded as the equivalent of pretangle neurons. More significantly, the density of AT8-positive neurons showed a significantly inverse or direct correlation with that of TUNEL-stained neurons in the frontal and CA regions. Uchihara et al [28] identified sequential changes in NFT antigenicity from AT8 to Gallyas positivity, in which Gallyas-unstained and AT8-labeled NFT were identified and diffusely AT8-labeled neurons largely corresponded to pretangle neurons. In this context, apoptosis defined as TUNEL positivity can occur in pretangle neurons, and regional differences in density of both TUNEL-stained and tau-labeled neurons may constitute supportive evidence for the occurrence of apoptosis at the pretangle neuron stage.

Studies both proving and disproving the co-localization of apoptosis and NFT have been published as neuropathological report and some of them indicate a lack of the typical apoptotic morphology in AD brains. Su et al [1], using the AT8 and PHF1 labeling and ISEL technique, failed to find a direct correlation between the phosphorylation site of tau protein and DNA fragmentation in the CA of AD. In contrast, Sugaya et al [9] reported a tendency for more strongly tau-labeled neurons to exhibit DNA fragmentation more frequently. And in a recent study [18], TUNEL-stained nuclei with normal morphology were more frequently associated with tau accumulation than were more severely damaged nuclei. A study using double labeling of ISEL and MN423, an anti-tau antiserum that recognizes tau molecules terminating at Glu-391 [22], reported a high frequency of co-localization of ISEL-positive DNA fragmentation and MN423-positive neurons, 61-79% of which showed DNA fragmentation. The authors speculated that tau molecule truncation was an important trigger of DNA fragmentation. Biochemical studies [24-25] reported that abnormal phosphorylation begins mainly in the neurites in the early stage of apoptosis, but that phosphorylated tau proteins are again dephosphorylated in the late stage. AT8 was identified as a marker for early phosphorylation sites of tau protein in AD and many AT8-positive neurons with TUNEL-unstained normal nuclei were observed. Therefore, the presence of such cells implies that the apoptotic process follows the initial phosphorylation but also that the apoptotic process may be reversible. This issue will be more precisely clarified by use of apoptosis-related proteins such as caspase-3 to localize apoptotic change because caspase-3 expression of neurons was shown to be closely associated with apoptotic change [15, 20, 24].

The frontal cortex and CA showed contrasting correlation for the density of TUNEL-stained nuclei and of neurons positive for AT8. The CA showed a higher density of Gallyas-stained NFT and AT8-positive neurons than did the frontal cortex. Because the CA and entorhinal cortex are an initial target region for NFT [34], necrotic neuronal change can be assumed to be the most drastic compared with the other cerebral lesions. The frontal cortex was affected lately by NFT and showed no correlation between the density of Gallyas-stained NFT and TUNEL-stained neurons, while HT7 expression showed more phosphorylation sites than that of AT8. This indicates that the scarcity of argyrophilic NFT and its relative abundance in pretangle neurons result in the significantly direct correlation in the frontal cortex. Bax and Bcl_2 were shown to be increased in NFT-free neurons and decreased after NFT formation [21]. Although it should be confirmed whether pretangle neurons show an increase in these two proteins, discrepancy between apoptosis and NFT formation might be explained by modulation with these two proteins.

The density of neurons positive for anti-tau antisera other than Tau2 generally indicated a predominant density of TUNEL-stained nuclei. This evidence suggests that abnormal phosphorylation of tau protein precedes apoptotic nuclear change. The high ratio of Tau2-positive neurons to TUNEL-stained nuclei is considered to be due to neuronal loss caused by late stage NFT because Tau2 tended to label typical tangle-shaped NFT. Amyloid fibril formation has been shown to be one factor associated with tau protein phosphorylation in AD [39], and early tau deposition is regulated by phosphorylated map kinase [16]. Apoptosis is essentially an intrinsic mechanism, so that factors (reviewed in [15]) merely accelerate or recover the process. Raina et al [24] introduced "abortosis"; a novel term that indicates avoidance or recovery from caspase-induced programmed cell death in AD. Early deposits of abnormally phosphorylated tau was shown to be related with AD7c-neuronal thread protein, and its gene regulate expression of this protein leading to neuronal cell death mediated by apoptosis [40-41]. These studies support our finding that apoptotic change follows phosphorylated tau protein deposits.

Acknowledgments

The authors wish to express their appreciation to Mr. Teruo Ikeda (Kanazawa University) and Ms. Eiko Yoshida (National Hokuriku Hospital) for their technical assistance. This study was supported by a grant-in-aid for Scientific Research (No. 11670937) from the Japanese Ministry of Education, Science and Culture.

References

1. Su JH, Anderson JA, Cummings BJ, Cotman CW. Immunohistochemical evidence of apoptosis in Alzheimer's disease. Neuroreport 1994; 5: 2529-2533.
2. Cotman CW, Anderson AJ. A potential role for apoptosis in neurodegeneration and Alzheimer's disease. Mol Neurobiol 1995; 10: 10-45.
3. Lassmann H, Bancher C, Breitschopf H, Wegiel J, Bobinski M, Jellinger KA, Wisniewski HM. Cell death in Alzheimer's disease evaluated by DNA fragmentation in situ. Acta Neuropathol (Berl) 1995; 89: 35-41.
4. Cotman CW, Su JH. Mechanisms of neuronal death in Alzheimer's disease. Brain Pathol 1996; 6: 493-506.
5. Smale G, Nichols NR, Brady DR, Finch CE, Horton WE Jr. Evidence for apoptotic cell death in Alzheimer's disease. Exp Neurol 1995; 133: 225-230.
6. Troncoso JC, Sukhov RR, Kawas CH, Koliatsos VE. In situ labeling of dying cortical neurons in normal ageing and Alzheimer's disease: correlations with senile plaques and disease progression. J Neuropathol Exp Neurol 1996; 55: 1134-1142.
7. Lucassen PJ, Chung WC, Kamphorst W, Swaab DF. DNA damage distribution in the human brain as shown by in situ end labeling; area-specific differences in ageing and Alzheimer's disease in the absence of apoptotic morphology. J Neuropathol Exp Neurol 1997; 56: 887-900.
8. Li WP, Chan WY, Lai HWL, Yew DT. Terminal dUTP nick end labeling (TUNEL) positive cells in the different regions of the brain in normal aging and Alzheimer patients. J Mol Neurosci 1997; 8: 75-82.
9. Sugaya K, Reeves M, McKinney M. Topographic associations between DNA fragmentation and Alzheimer's disease neuropathology in the hippocampus. Neurochem Int 1997; 31: 275-281.
10. Sheng JG, Mrak RE, Griffin WST. Progressive neuronal DNA damage associated with neurofibrillary tangle formation in Alzheimer's disease. J Neuropathol Exp Neurol 1998; 57: 323-328
11. Sheng JG, Xue QZ, Mrak RE, Griffin WST. Progressive neuronal injury associated with amyloid plaque formation in Alzheimer disease. J Neuropathol Exp Neurol 1998; 57: 714-717
12. Jellinger KA, Bancher C. Neuropathology of Alzheimer's disease: a critical update. J Neural Transm (Suppl) 1998; 54: 77-95.
13. Stadelmann C, Bruck W, Bancher C, Jellinger KA, Lassmann H. Alzheimer's disease: DNA fragmentation indicates increased neuronal vulnerability, but not apoptosis. J Neuropathol Exp Neurol 1998; 57: 456-464.
14. Selkoe DJ. Translating cell biology into therapeutic advances in Alzheimer's disease. Nature 1999; 399 (Suppl): A23-31.
15. Behl C. Apoptosis and Alzheimer's disease. J Neural Transm 2000; 107: 1325-1344.
16. Ferrer I, Blanco R, Carmona M, Ribera R Goutan E, Puig B, Rey MJ, Cardozo A, Vinalis F, Ribalta T. Phosphorylated map kinase (ERK1, ERK2) expression is associated with early tau deposition in neurons and glial cells, but not with increased nuclear DNA vulnerability and cell death, in Alzheimer disease, Pick's disease,

progressive supranuclear palsy and corticobasal degeneration. Brain Pathol 2001; 11: 144-158.
17. Ferrer I, Puig B, Krupinsk J, Carmona M, Blanco R. Fas and Fas ligand expression in Alzheimer's disease. Acta Neuropathol (Berl) 2001; 102: 121-131.
18. Broe M, Schepherd CE, Milward EA, Halliday GM. Relationship between DNA fragmentation, morphological changes and neuronal loss in Alzheimer's disease and dementia with Lewy bodies. Acta Neuropathol (Berl) 2001; 101: 616-624.
19. Ugolini G, Cattaneo A, Novak M. Co-localization of truncated tau and DNA fragmentation in Alzheimer's disease neurons. Neuroreport 1997, 8: 3709-3712.
20. Nagy Z, Esiri MM. Apoptosis-related protein expression in the hippocampus in Alzheimer's disease. Neurobiol Aging 1997; 18: 565-571.
21. Giannakopoulos P, Kovari E, Savioz A, De Bilbao F, Dubois-Dauphin M, Hof PR, Bouras C. Differential distribution of presenilin-1, Bax, and Bcl-X_l in Alzheimer's disease and frontotemporal dementia. Acta Neuropathol (Berl) 1999; 98: 141-149.
22. Shirley BS, Johnson GV. Tau and HMW tau phosphorylation and compartmentalization in apoptotic neuronal PC12 cells. J Neurosci Res 2001; 66: 203-213.
23. Mookherjee P, Johnson GV. Tau phosphorylation during apoptosis of human SH-SY5Y neuroblastoma cells. Brain Res 2001; 921: 31-43.
24. Raina AK, Hochman A, Zhu X, Rottkamp CA, Numomura A, Siedlak SL, Boux H, Castellani RJ, Perry G, Smith MA. Abortive apoptosis in Alzheimer's disease. Acta Neuropathol (Berl) 2001; 101: 305-310.
25. Kobayashi K, Hayashi M, Nakano H, Fukutani Y, Sasaki K, Shimazaki M, Koshino Y. Apoptosis of astrocytes with enhanced lysosomal activity and oligodendrocytes in white matter lesions in Alzheimer's disease. Neuropathol Appl Neurobiol 2002; 28: 238-251.
26. Bancher C, Brunner C, Lassmann H, Budka H, Jellinger K, Wiche G, Seiterberger F, Grundke-Iqbal I, Iqbal K, Wisniewski HM. Accumulation of abnormally phosphorylated tau precedes the formation of neurofibrillary tangles in Alzheimer's disease. Brain Res 1989; 477: 90-99.
27. Braak E, Braak H, Mandelkow EM. A sequence of cytoskeletal changes related to the formation of neurofibrillary tangles and neuropil threads. Acta Neuropathol (Berl) 1994; 87: 554-567.
28. Uchihara T, Nakamura A, Yamazaki M, Mori O. Evolution from pretangle neurons to neurofibrillary tangles monitored by thiazin red combined with Gallyas method and double immunofluorescence. Acta Neuropathol (Berl) 2001; 101: 535-539.
29. Kimura T, Ono T, Takamatsu J Yamamoto H, Ikegami K, Kondo A, Hasegawa M, Ihara Y, Miyamoto E, Miyakawa T. Sequential changes of tau-site-specific phosphorylation during development of paired helical filaments. Dementia 1996; 7: 177-181.
30. Su JH, Cummings BJ, Cotman CW. Early phosphorylation of tau in Alzheimer's disease occurs at Ser-202 and is preferentially located within neurites. Neuroreport 1994; 5: 2358-2362.
31. Mercken M, Vandermeeren M, Lübke U, Six J, Boons J, Van de Voorde A, Martin JJ, Gheuens J. Monoclonal antibodies with selective specificity for Alzheimer tau are

directed against phosphatase-sensitive epitopes. Acta Neuropathol (Berl) 1992; 84: 265-272.
32. Szendrei GI, Lee VM-Y, Otvos L. Recognition of the minimal epitope of monoclonal antibody tau-1 depends upon the presence of a phosphate group but not its location. J Neurosci Res 1993; 34: 243-249.
33. Papasozomenos SC. Tau protein immunoreactivity in dementia of the Alzheimer type: II. Electron microscopy and pathogenetic implications. Effects of fixation on the morphology of the Alzheimer's abnormal filaments. Lab Invest 1989; 60: 375-389.
34. Dickson DW, Ksiezak-Reding H, Liu WK, Davies P, Crowe A, Yen SH. Immunocytochemistry of neurofibrillary tangles with antibodies to subregions of tau protein: identification of hidden and cleaved tau epitopes and a new phosphorylation site. Acta Neuropathol (Berl) 1992; 84: 596-605.
35. Mirra SS, Heyman A, McKeel D, Sumi SM, Crain BJ, Brownlee LM, Vogel FS, Hughes JP, van Belle G, Berg L, and participating CERAD neuropathologists. The Consortium to Establish a Registry for Alzheimer's disease (CERAD). Part II. Standardization of the neuropathologic assessment of Alzheimer's disease. Neurology 1991; 41: 479-486.
36. Khachaturian ZS. Diagnosis of Alzheimer's disease. Arch Neurol 1985; 42: 1097-1105.
37. Braak H, Braak E. Neuropathological stageing of Alzheimer-related changes. Acta Neuropathol (Berl) 1991; 82: 239-259.
38. Anderson AJ, Stoltzner S, Lai F, Su J, Nixon RA. Morphological and biochemical assessment of DNA damage and apoptosis in Down syndrome and Alzheimer disease, and effect of postmortem tissue archival on TUNEL. Neurobiol Aging 2000; 21: 511-524.
39. Busciglio J, Lorenzo A, Yeh J, Yankner BA. β -Amyloid fibrils induces tau phosphorylation and loss of microtubule binding. Neuron 1995; 14: 879-888.
40. de la Monte SM, Carlson RI, Brown NV, Wands JR. Profiles of neuronal threads protein expression in Alzheimer's disease. J Neuropathol Exp Neurol 1996; 55: 1038-1050.
41. de la Monte SM, Wands JR. Alzheimer-associated neuronal threads protein-induced apoptosis and impaired mitochondrial function in human central nervous system-derived neuronal cells. J Neuropathol Exp Neurol 2001; 60: 195-207.

Legend

Figure 1
(a) Double labeling of AT8 and TUNEL of the frontal cortex (X400). AT8-positive tangle-like structures (black arrows) are seen in the neuronal cytoplasm with TUNEL-stained nuclei. A TUNEL-stained nucleus without AT8-positive structure is indicated with the white arrow. (b) Double labeling of AT180 and TUNEL of the CA (X400). Apoptotic bodies are indicated with the arrow. AT180 frequently labeled neuropil threads, and the labeled neuron lacks fine structures of the nucleus. (c) Double labeling of HT7 and TUNEL of the cingulate cortex (X720). HT7-positve and TUNEL-stained neurons (black arrows) show almost normal nuclei, and HT7 labels homogeneously the neuronal cell body.

Figure 2
The density of labeled neurons (/0.00168mm^2) of the seven cerebral regions. Error bars indicate standard deviation.

Figure 3
Percentile values of ratio of neurons labeled with TUNEL to those labeled with other methods.
The percentile values of ratio of TUNEL to Tau2 are higher than those of TUNEL to other labeling.

Table 1
The results of two-tailed Student's t-test of the density of the labeled neurons by different labeling. The open boxes for statistically significant t values and the shaded box for insignificant t values. P indicates statistical probability and significance is set at $p<0.05$.

TUNEL

	CA	Cingulate	Temporal	Frontal	Parietal	Occipital
Entorhinal	t=2.22, p=0.0304	t=5.337, p<0.0001	t=3.090, p=0.0031	t=5.988, p<0.0001	t=1.322, p=0.1933	t=2.243, p=0.0302
Cingulate	t=5.645, p<0.0001					
Temporal	t=1.546, p=0.1275	t=2.210, p=0.0310				
Frontal	t=8.646, p<0.0001	t=8.821, p<0.0001	t=4.734, p<0.0001			
Parietal	t=0.368, p=0.715	t=4.746, p<0.0001	t=1.373, p=0.1771	t=6.891, p<0.0001		
Occipital	t=1.175, p=0.2466	t=3.233, p=0.001	t=0.294, p=0.7705	t=7.138, p<0.0001	t=1.164, p=0.2548	

AT8

	CA	Cingulate	Temporal	Frontal	Parietal	Occipital
Entorhinal	t=-0.725, p=0.4712	t=-6.166, p<0.0001	t=4.595, p<0.0001	t=8.059, p<0.0001	t=6.920, p<0.0001	t=3.025, p=0.0048
Cingulate	t=5.620, p<0.0001					
Temporal	t=3.923, p=0.0002	t=-2.060, p=0.0439				
Frontal	t=7.537, p<0.0001	t=2.019, p=0.0486	t=-4.196, p<0.0001			
Parietal	t=6.402, p<0.0001	t=0.871, p=0.3883	t=-2.947, p<0.0001	t=-1.155, p=0.2534		
Occipital	t=2.758, p=0.0094	t=-0.484, p=0.6318	t=-6.720, p<0.0001	t=-1.541, p=0.1329	t=0.993 p=0.3293	

Gallyas

	CA	Cingulate	Temporal	Frontal	Parietal	Occipital
Entorhinal	t=-0.541, p=0.5903	t=-1.911, p=0.0610	t=4.673, p<0.0001	t=8.754, p<0.0001	t=4.352, p<0.0001	t=3.856, p=0.0003
Cingulate	t=1.316, p=0.1932					
Temporal	t=3.550, p=0.0007	t=1.648, p=0.1043				
Frontal	t=6.727, p<0.0001	t=4.125, p=0.0001	t=-3.139, p=0.0025			
Parietal	t=3.018, p=0.0038	t=1.028, p=0.3082	t=0.930, p=0.3557	t=-4.838, p<0.0001		
Occipital	t=2.784, p=0.0072	t=0.992, p=0.3253	t=-3.119, p=0.0035	t=-4.090, p=0.0001	t=-0.050, p=0.9606	

AT180

	CA	Cingulate	Temporal	Frontal	Parietal	Occipital
Entorhinal	t=1.394, p=1687	t=-5.186, p<0.0001	t=2.984, p=0.0042	t=6.639, p<0.0001	t=7.922, p<0.0001	t=8.729, p<0.0001
Cingulate	t=5.530, p<0.0001					
Temporal	t=3.836, p=0.0003	t=-2.696, p=0.0094				
Frontal	t=6.812, p<0.0001	t=1.721, p=0.0917	t=-4.412, p<0.0001			
Parietal	t=7.866, p<0.0001	t=1.742, p=0.0874	t=-5.130, p<0.0001	t=-0.376, p=0.7088		
Occipital	t=7.174, p<0.0001	t=3.349, p=0.0020	t=-6.720, p<0.0001	t=1.417, p=0.1659	t=-2.388, p=0.0220	

HT7

	CA	Cingulate	Temporal	Frontal	Parietal	Occipital
Entorhinal	t=0.512, p=0.618	t=-1.456, p=0.1512	t=0.429, p=0.6709	t=1.640, p=0.1070	t=4.047, p=0.0002	t=4.509, p<0.0001
Cingulate	t=1.717, p=0.0918					
Temporal	t=0.851, p=0.3985	t=-0.959, p=0.3418				
Frontal	t=1.871, p=0.0668	t=0.396, p=0.6936	t=-1.229, p=0.2244			
Parietal	t=3.949, p=0.0002	t=1.900, p=0.0629	t=-2.947, p<0.0001	t=1.046, p=0.3003		
Occipital	t=3.838, p=0.0005	t=2.585, p=0.0143	t=-3.454, p=0.0014	t=1.579, p=0.1239	t=-1.767 p=0.0853	

Tau2

	CA	Cingulate	Temporal	Frontal	Parietal	Occipital
Entorhinal	t=-0.040, p=0.9683	t=-1.615, p=0.1130	t=3.922, p=0.0002	t=1.931, p=0.0589	t=4.748, p<0.0001	t=3.718, p=0.0007
Cingulate	t=1.357, p=0.1811					
Temporal	t=3.009, p=0.0039	t=0.882, p=0.3812				
Frontal	t=1.702, p=0.0945	t=0.378, p=0.7071	t=0.326, p=0.7458			
Parietal	t=3.609, p=0.0007	t=1.622, p=0.1114	t=-1.298, p=0.1994	t=1.091, p=0.2802		
Occipital	t=2.206, p=0.0344	t=0.695, p=0.4919	t=-0.248, p=0.8053	t=1.579, p=0.1239	t=0.707 p=0.4846	

Tau5

	CA	Cingulate	Temporal	Frontal	Parietal	Occipital
Entorhinal	t=0.832, p=0.4087	t=-1.942, p=0.0574	t=0.956, p=0.3429	t=2.689, p=0.0098	t=4.266, p<0.0001	t=3.542, p=0.0011
Cingulate	t=2.686, p=0.0096					
Temporal	t=1.784, p=0.0796	t=-1.078, p=0.2895				
Frontal	t=3.329, p=0.0016	t=0.966, p=0.3387	t=-1.943, p=0.0573			
Parietal	t=4.998, p<0.0001	t=2.171, p=0.0345	t=-3.420, p=0.0012	t=0.703, p=0.4851		
Occipital	t=3.914, p=0.0004	t=2.384, p=0.0230	t=-3.119, p=0.0035	t=1.579, p=0.1239	t=-1.047, p=0.3017	


1a

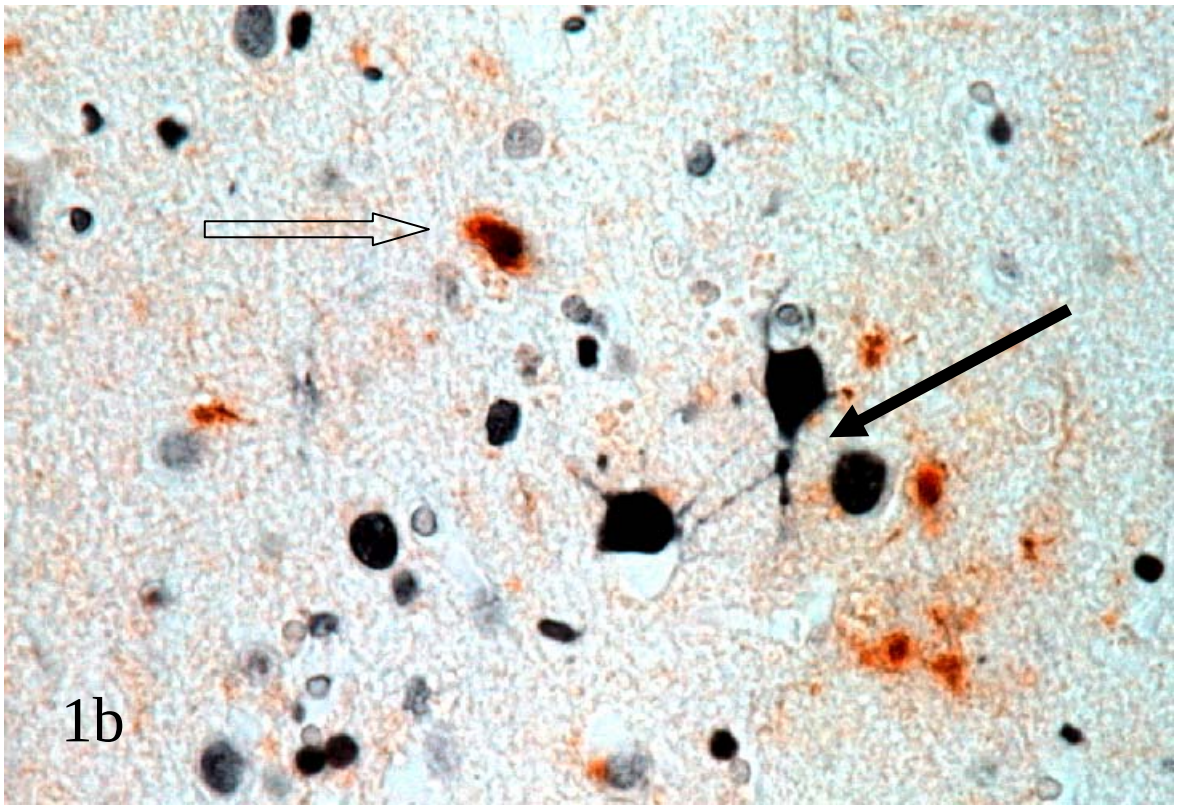
1b

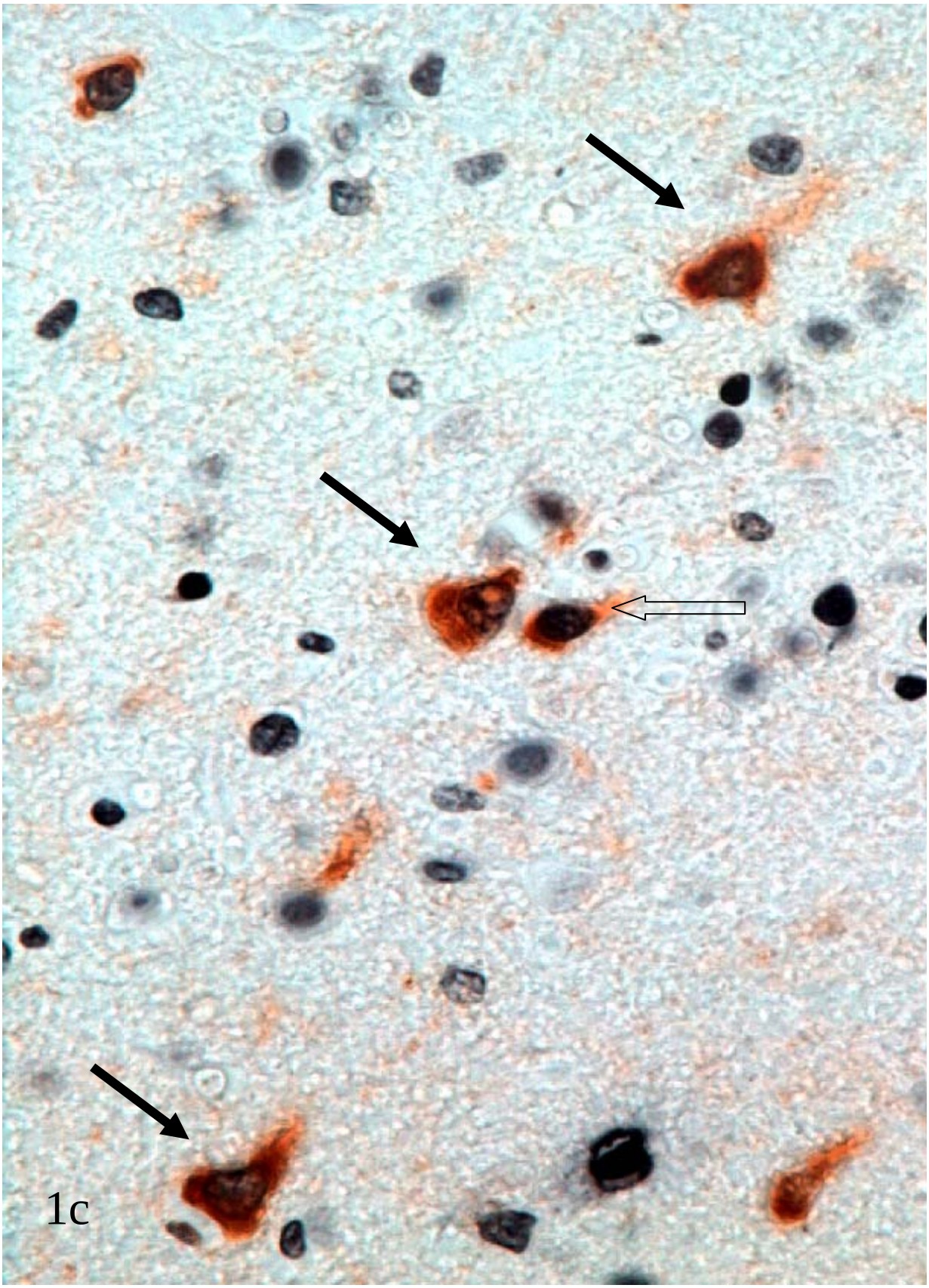
1c

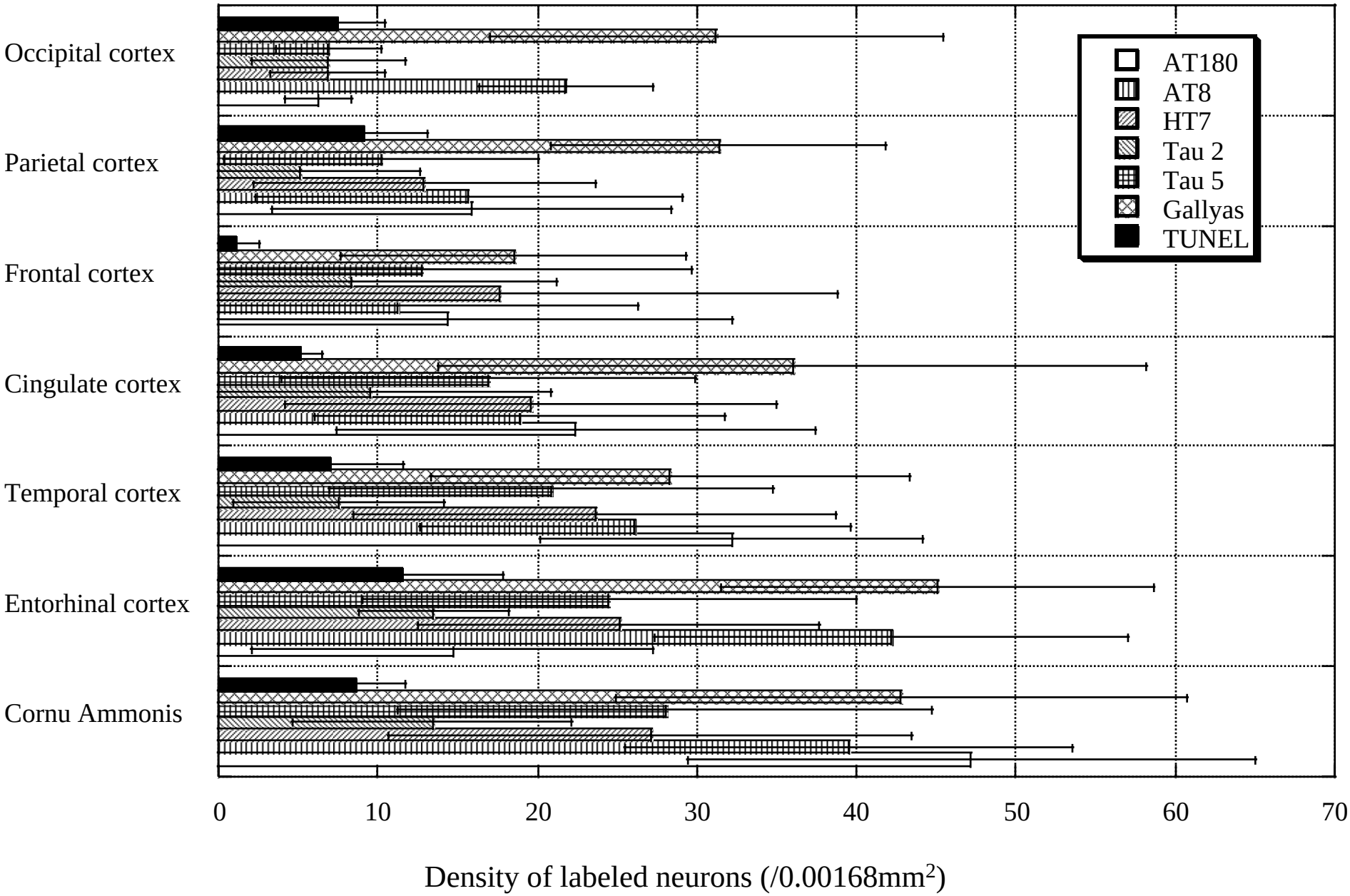
Occipital cortex
Parietal cortex
Frontal cortex
Cingulate cortex
Temporal cortex
Entorhinal cortex
Cornu Ammonis
AT180
AT8
HT7
Tau 2
Tau 5
Gallyas
TUNEL
0
10
20
30
40
50
60
70
Density of labeled neurons (/0.00168mm2)

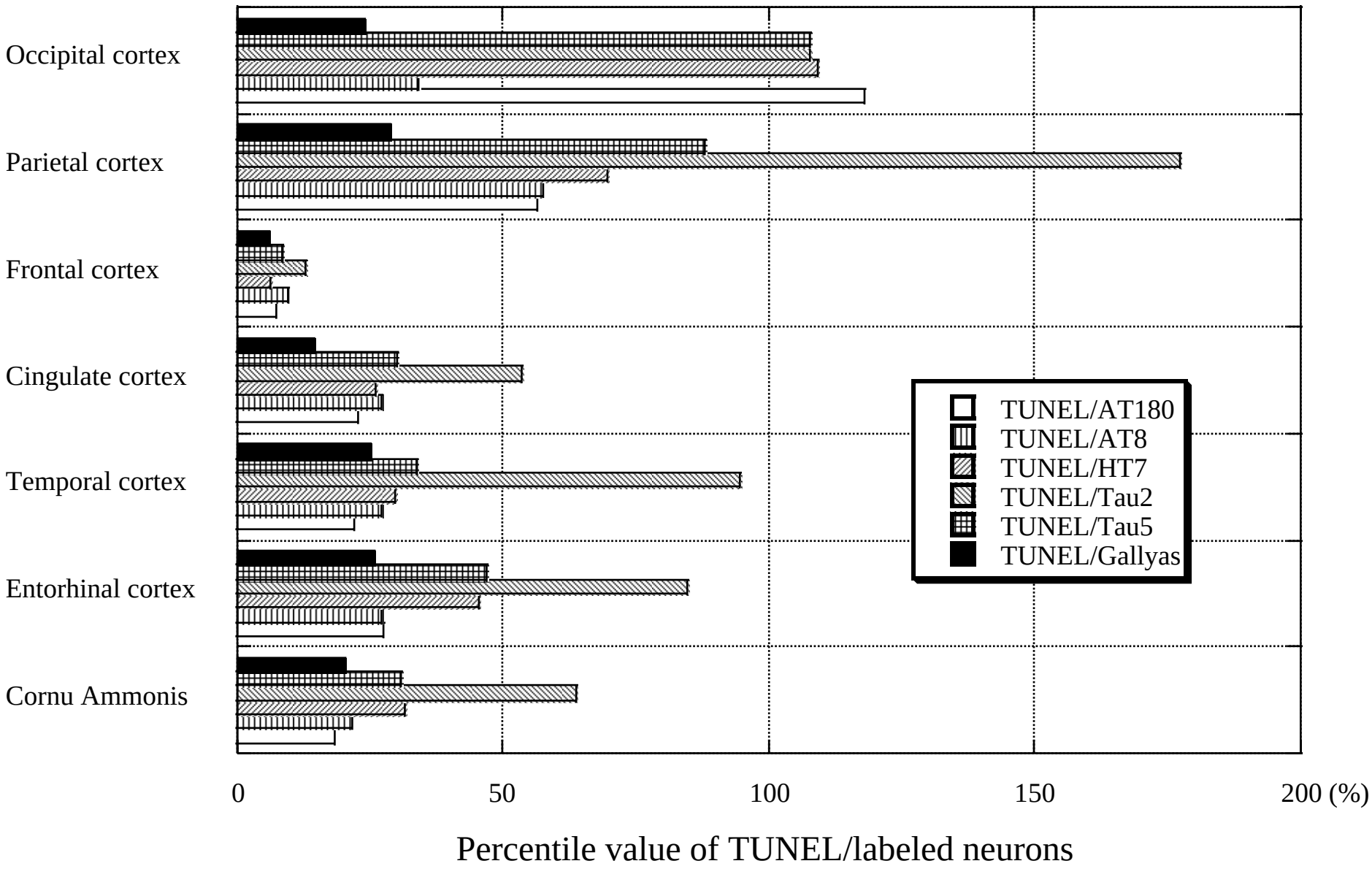
Occipital cortex
Parietal cortex
Frontal cortex
Cingulate cortex
Temporal cortex
Entorhinal cortex
Cornu Ammonis
TUNEL/AT180
TUNEL/AT8
TUNEL/HT7
TUNEL/Tau2
TUNEL/Tau5
TUNEL/Gallyas
0
50
100
150
200 (%)
Percentile value of TUNEL/labeled neurons